A study of the relationship between coulombic efficiency and capacity degradation of commercial lithium-ion batteries

Fangfang Yang [a, *], Dong Wang [a], Yang Zhao [a], Kwok-Leung Tsui [a], Suk Joo Bae [b]

[a] *Department of Systems Engineering and Engineering Management, City University of Hong Kong, Hong Kong*
[b] *Department of Industrial Engineering, Hanyang University, Seoul 04763, South Korea*

ARTICLE INFO

ABSTRACT

High coulombic efficiency (CE) usually indicates a long battery cycle life. However, the relationship between long-term CE evolution and battery degradation is not fully understood yet. This paper explores the behavior of long-term CE and clarifies its relationship with capacity degradation. Cycle life tests are conducted on two types of mainstream commercial lithium-ion batteries. An incremental capacity (IC) analysis is then employed to identify battery aging mechanisms. Experimental observations along with in-depth discussions are presented regarding battery degradation, aging mechanisms, and CE evolution. From the experimental results, two typical degradation patterns are recognized. From the IC analysis, we observed that, in addition to a loss of lithium inventory, a loss of active material accelerates battery degradation and brings down CE values. From an electrochemical perspective, this paper establishes the relationship between CE evolution and capacity degradation. This relationship can help develop battery degradation models, estimate battery health states, and provide early failure warnings for a battery management system.

© 2017 Elsevier Ltd. All rights reserved.

1. Introduction

Owing to high energy density, high power density, long cycle life, and free of memory effects, lithium-ion batteries have been extensively used as one of main energy sources for portable electronics (e.g., cameras, laptops, and cellular phones) and electric transportation (e.g., electric vehicles and hybrid electric vehicles) [1]. Nonetheless, as with most battery systems, lithium-ion batteries suffer from capacity and power fade during repeated charge-discharge processes. It was found that the performance loss of lithium-ion batteries mainly attributes to three aging processes: the loss of lithium inventory (LLI), loss of active material (LAM), and an increase in internal resistance (IR), amongst which the LLI, caused by side reactions, was identified as the main source of performance fade [2]. Side reactions, including the formation and growth of a solid electrolyte interface (SEI) film, electrolyte decomposition, passivation, metallic lithium plating and subsequent corrosion, and gas evolution, always take place at an interface between the electrolyte and electrodes [3].

Coulombic efficiency (CE), as a battery parameter to monitor the magnitude of side reactions, has been of great interest in recent years [4]. CE is defined as:

$$\eta = \frac{C_d}{C_c}, \tag{1}$$

where C_d is the discharge capacity of a cell at a single cycle, and C_c is the charge capacity of the cell in the same cycle. Theoretically, when a cell is free of undesired side reactions, its CE should be 1.000 permanently, indicating the cell will operate forever [4]. The relationships between CE and other battery parameters, e.g., battery lifetime, state of charge, current rate, and operating temperature, have been widely reported. Ohzuku et al. [5], Gyenes et al. [6], and Burns et al. [7] reported the relationship between CE and battery lifetime, and suggested that accurate measurements of CE can help promptly estimate the lifetime of lithium-ion cells. Ng et al. [8] and Zheng et al. [9] showed the correlation between SOC and CE, and claimed that CE is almost invariant with SOC changes. Other existing works reported the correlations between CE, current rate [10], operating temperature [4], etc. Besides, some authors focused on the measurement of CE and reported that precise CE

* Corresponding author.
E-mail addresses: fangfyang2-c@my.cityu.edu.hk (F. Yang), dongwang4-c@my.cityu.edu.hk (D. Wang), yangzhao9-c@my.cityu.edu.hk (Y. Zhao), kltsui@cityu.edu.hk (K.-L. Tsui), sjbae@hanyang.ac.kr (S.J. Bae).

measurements are extremely difficult to obtain, subject to current sensors precision [9,11] and channel-to-channel variation [12].

Nonetheless, rare research works have investigated the relationship between CE and battery degradation. Most existing literature focused on CE of initial 100−200 cycles and then evaluated the correlations between CE and other factors with an averaged CE value. In general, the degradation process of a lithium-ion battery includes multiple stages, such as two-stage degradation [13] and three-stage degradation [2]. Thus, using an averaged CE value to evaluate the relationship between CE and battery lifetime could be inappropriate. For those studies on long-term CE behaviors, the emphasis was laid mostly on the understanding of specific/anomalous behaviors, such as an increase of CE at initial cycles [14,15] and a value of CE exceeding 1.0 [6]. To the best of our knowledge, the behaving pattern of CE over cycle life and its relationship with battery aging has not been fully explored.

In this paper, two mainstream commercial lithium-ion batteries, including a lithium iron phosphate (LFP) battery (power support for plug-in vehicles of BYD, a Chinese automaker) and a nickel manganese cobalt oxide (NMC) battery (used in Tesla's grid battery), are used to investigate long-term cycling behaviors. We chose these two battery types because: 1) these two batteries are commercially popular in industrial applications; 2) they exhibit two representative capacity degradation behaviors which are commonly observed in the degradation of lithium-ion batteries [13]. We first study the aging behavior of these two lithium-ion batteries, with a focus on their capacity degradation, CE evolution, and incremental capacity (IC) curves. As capacity is one of the leading battery performance indicators, a long-term capacity degradation behavior is examined to study the effects of CE on battery degradation. Moreover, the understanding of battery degradation mechanisms helps us better correlate CE with battery degradation. Hence, IC analysis, as a non-destructive method, is employed to analyze the aging mechanisms of lithium-ion batteries. We then investigate the relationships among CE, capacity degradation, and the aging process inside a single cell under a long-term cycle life test.

The rest of this paper is organized as follows. Section 2 illustrates the experimental setups of battery aging tests. The aging performances including capacity degradation, CE evolution, and aging mechanism analyzed by an IC curve are then presented in Section 3. Section 4 presents the summary and discussions of the aforementioned relationship and finally conclusions are drawn in Section 5.

2. Experiments

Two commercial cylindrical lithium-ion cells including LiFePO$_4$ (LFP) 18650HP-Fe cells (type A) and Li(NiMnCo)O$_2$ (NMC) B18650CD cells (type B) from the BAK Company were used in our experiments. The specifications of the LFP and NMC cells are tabulated in Table 1. Three cells of the same type were tested using an Arbin BT2000 battery tester on a test bench described in Ref. [16]. In our experiments, all cells were respectively placed in a climatic chamber (Votsch VC^3 7100) and a temperature of 45°C was maintained for the battery life cycle tests. Each life cycle consisted of a 1C charge process under a constant-current/constant-voltage (CC/CV) mode and a 1C discharge process. For example, the input
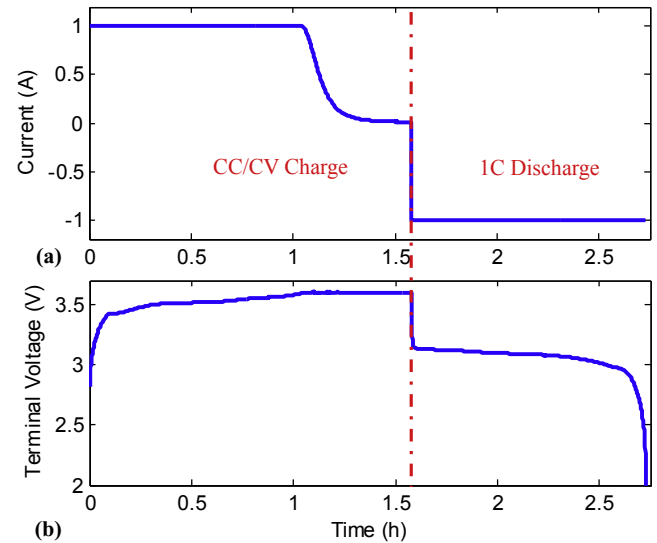

Fig. 1. Current (a) and terminal voltage (b) profiles of a charge-discharge life cycle of an LFP cell.

current and measured terminal voltage profiles of a life cycle of an LFP cell are plotted in Fig. 1 (a) and (b), respectively.

3. Results and observations

3.1. Capacity evolution of the LFP cells and the NMC cells

Battery performance degrades over repeated charge-discharge cycles. Performance degradation can be reflected by some battery parameters, such as capacity, IR, AC impedance, self-discharge rate, and power density [17]. Among them, capacity, representing specific energy in ampere-hours, is a leading battery performance indicator [18]. Mathematically, it is evaluated by integrating current over time. To compare the degradation behavior of the two different cells, normalized capacity, which is also named as state-of-health (SOH) and is defined as the ratio of the current capacity to its initial maximum deliverable capacity, is adopted in this paper.

Two distinct degradation patterns are observed from our experimental results. The degradation traces of LFP and NMC cells are shown in Fig. 2 (a) and Fig. 3 (a), respectively, while the degradation rates of all subjects, approximated by the average capacity drop of every 100 cycles, are plotted in Fig. 2 (b) and Fig. 3 (b), respectively. In Fig. 2 (a), the degradation curves of LFP cells have a typical convex shape (intuitively, the bowl shape). In the initial cycles of Fig. 2 (a), their capacities experience a sharp decreasing phase, and then they maintain a relatively slow degradation rate over a wide range of cycles. The capacity degradation rates decrease slowly as cycle number increases, as shown in Fig. 2 (b). Considering Cell A2, for example, about 20% of a nominal capacity is lost in the first 1000 cycles, while only about 15% is lost during the following 1000 cycles. NMC cells in Fig. 3 (a), in contrast, exhibit a two-phase concave degradation behavior. An inflection point representing the transition between the two phases can be

Table 1
Specifications of LFP and NMC cells.

Type	Cathode material	Anode material	Nominal capacity (Ah)	Nominal voltage (V)	Upper cut-off voltage (V)	Lower cut-off voltage (V)
A	LFP	Graphite	1	3.2	3.6	2
B	NMC	Si/C	1.3	3.6	4.2	2.5
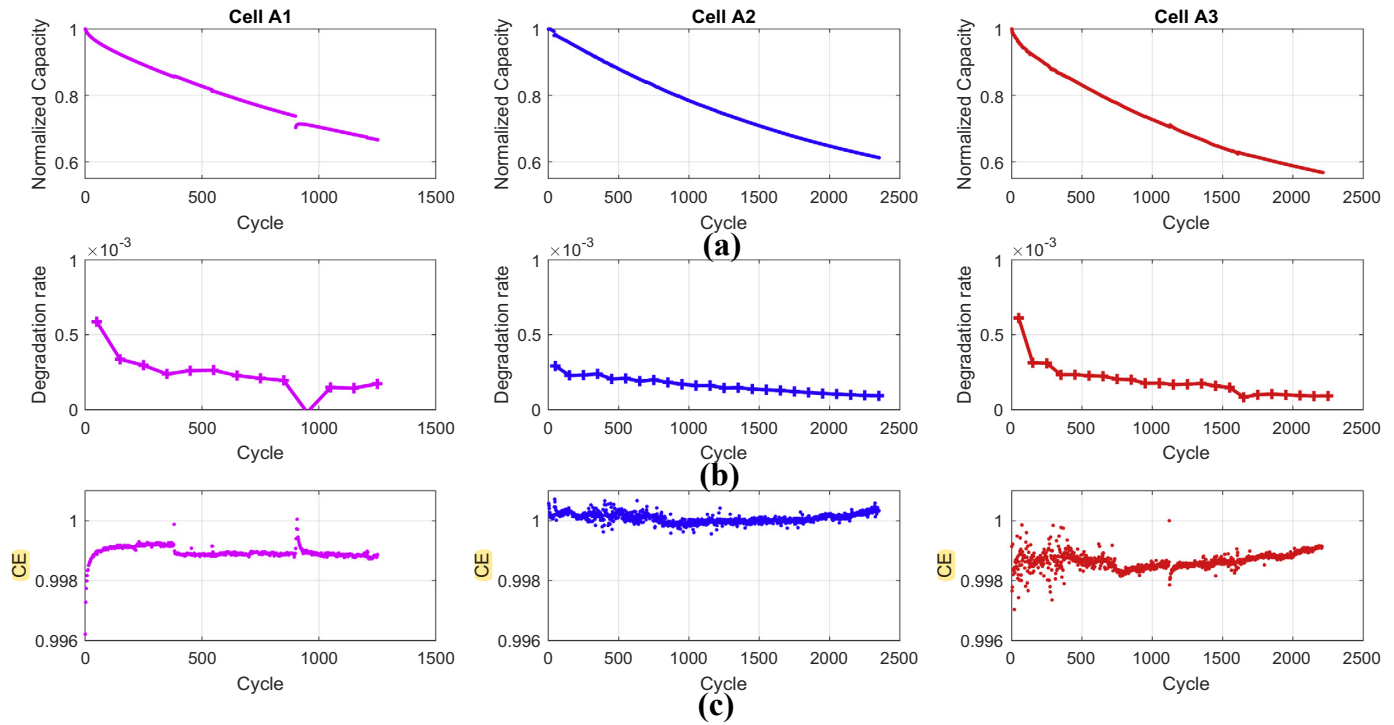
Fig. 2. Normalized capacity vs. cycle number (a), capacity degradation rate vs. cycle number (b), and CE vs. cycle number (c) for LFP cells cycled at 45°C and a discharge rate of 1C.
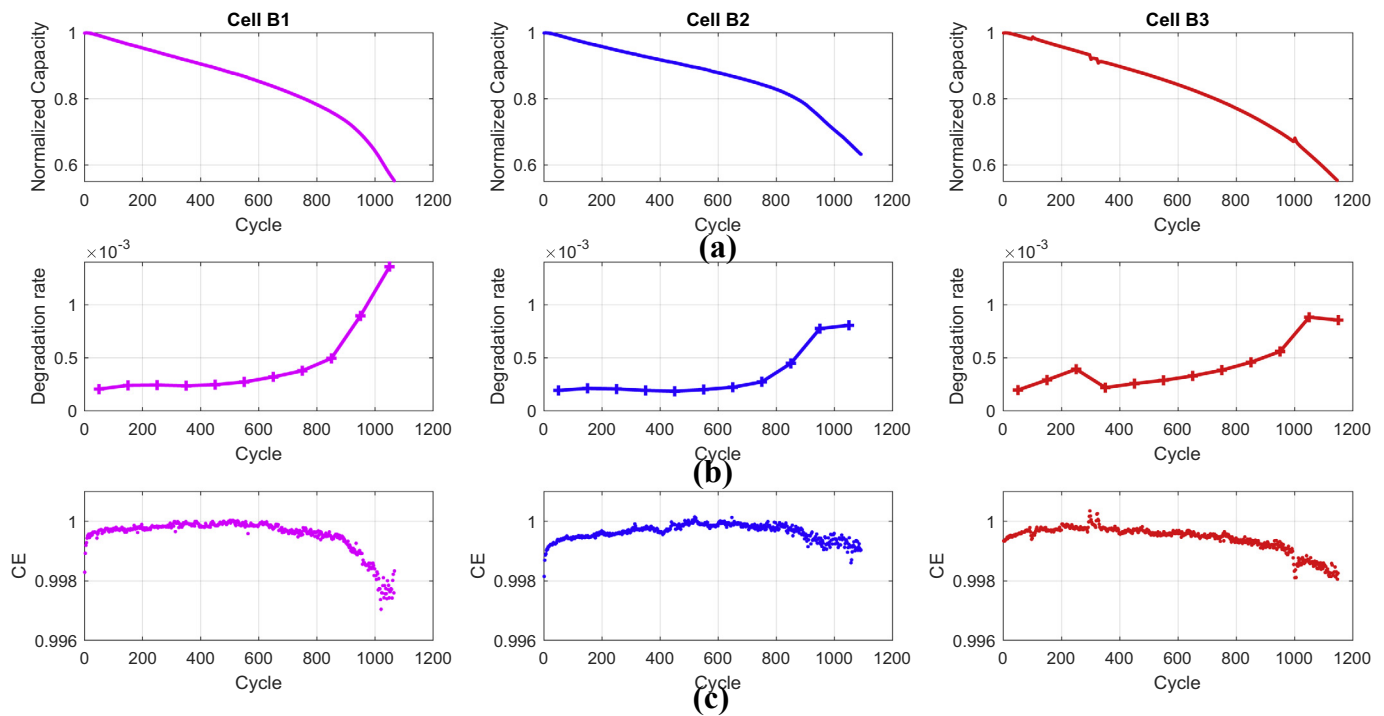
Fig. 3. Normalized capacity vs. cycle number (a), capacity degradation rate vs. cycle number (b), and CE vs. cycle number (c) for NMC cells cycled at 45°C and a discharge rate of 1C.

clearly observed in the degradation paths of NMC cells in Fig. 3 (a). The capacity degrades slowly during the first couple of hundred cycles. After the inflection point, the degradation rates of NMC cells begin to increase dramatically, as shown in Fig. 3 (b). After a 20% decrease of nominal capacities, the degradation rates of NMC cells are faster than those of LFP cells. The difference in the degradation

patterns has very different effects on the cycle life of a battery, which is defined as the number of complete charge/discharge cycles before its capacity drops below 80% of its nominal value [19]. For instance, the average cycle life of LFP cells is 698 cycles in our experiment, while in contrast, the average cycle life of NMC cells is 784 cycles, which is significantly longer. Nevertheless, it takes

another 1500 cycles for the capacity of LFP cells to drop from 80% to 60%, while the same value for NMC cells is less than 500 cycles.

The two distinct capacity degradation behaviors have been commonly observed in the degradation process of lithium-ion batteries. The convex degradation pattern has been found in Refs. [20–22], while the two-stage concave degradation pattern has been found in Refs. [2,23,24]. It is worth noting that an NMC cell may exhibit a convex shape of capacity degradation, and vice versa, owing to the highly confidential design and manufacturing process of commercial batteries (e.g., electrode design and VC additive, electrolyte composition, impurities, etc.)

3.2. Coulombic efficiency for battery degradation assessment

In this section, we focus on the investigation of the effectiveness of CE with respect to the degradation of battery capacity. CE of a cell at cycle k is defined as the ratio of the delivered capacity during discharge at cycle k, $C_{d,k}$, to the stored capacity during charge at the same cycle, $C_{c,k}$ as [21]:

$$\eta_k = \frac{C_{d,k}}{C_{c,k}} = \frac{\int_0^{t_{d,k}} i_d dt}{\int_0^{t_{c,k}} i_c dt},\qquad(2)$$

where i_d and i_c are currents during discharge and charge processes, respectively; $t_{d,k}$ and $t_{c,k}$ are time durations during discharge and charge processes at cycle k, respectively. CE depicts the completeness of the electron transfer between charge and discharge processes in an electrochemical system.

Fig. 2 (c) and Fig. 3 (c) respectively show the CEs of LFP and NMC cells from repeated charge-discharge cycles. The sampling interval is 5s, and the current resolution is 0.0015% FSR. The CE value ranges from 0.996 to 1.001, and contains a degree of noise and scatter over a range of approximately ±0.02%. Compared with the capacity data, CE, as a ratio of two close capacities, is more sensitive to uncontrollable external conditions such as unpredicted power off and recovery, surface and internal temperature variations of cells, and the stability of contacts to cells. Nevertheless, this level of precision is adequate for us to study a long-term CE behavior.

For most of the cells, there is a sharp CE increase in initial cycles, and then it is relatively stable for several hundreds of cycles. This is because for a fresh battery, "sufficient" time is required for the formation of an SEI film on the surface of electrode particles [1]. Additionally, in some cases, such as Cell A2, calculated CEs exceed 1.000 and last for several consecutive cycles. The same phenomenon has been observed in Ref. [6], where it is explained as the impact of lithium atoms stored in the anode "overhang".

It is obvious that CE evolution curves of LFP and NMC cells have quite different patterns. For NMC cells, there is a descending trend at the tail of CE curves, however, such trends are not visible for LFP cells. CE evolution trends of NMC cells are of a bow shape. It first increases to a steady state in the first several cycles, then maintains at that level for hundreds of cycles, finally, after a certain point, decreases significantly. Taking Cell B1 in Fig. 3 (c) for example, CE goes up to a steady value for the first 50 cycles, then remains relatively stable until the 900th cycle. Thereafter, CE begins to decline at a noticeable speed. Recalling the concave degradation trend of Cell B1 in Fig. 3 (a), an inflection point separating the slow and fast degradation phases is located around the 900th cycle. Numerically, the two values are consistent, which is not a mere coincidence. In fact, more correlations have been identified between CE curves and the capacity degradation rate. The slight ascending trends at the CE curve tails are observed for Cells A2 and

A3, corresponding to a slower degradation rate in Fig. 2 (b). In contrast, the sharp decreases in the CE values of NMC cells are observed in Fig. 3 (c), coinciding with the rapid capacity degradation rate presented in Fig. 3 (b).

As for the same type of batteries, after stabilizing, a cell with higher CE usually has a longer cycle life. For example, Cell A2 with an average CE of 0.9999 has the longest cycle life among the LFP cell trends plotted in Fig. 2. For NMC cells, in Fig. 3, Cell B2 has higher CE curves than those of Cells B1 and B3, it also has a longer cycle life according to Fig. 3 (a). For this qualitative relationship to work, some issues need to be carefully considered. First, cycles needed to reach a steady CE value which varies a lot for different batteries. From our test subjects, it takes less than 100 cycles for LFP cells to reach the steady CE value; in contrast, NMC cells usually take more than 300 cycles. What is more, as a result of CE sensitivity and channel-to-channel variation [12], the CE value fluctuates within a certain range. Subsequently, it would be more reliable to consider the mean CE value of a few consecutive cycles. Additionally, for different cells, lower CE does not always mean a faster degradation rate. It can be observed from Fig. 2 (b) and (c), after Cycle 1000, Cells A2 and A3 have almost the same degradation rate, but their CE values are different. A similar phenomena have been reported by Deshpande et al. [15] and Xu et al. [14].

In this section, we have investigated the properties of CE as a battery indicator, in terms of battery capacity degradation. Our experimental results suggest that CE evolution is distinct for different types of batteries. Moreover, the strong correlation between a steady CE value and a battery cycle life has been detected at the same type of cells. More importantly, we have observed that, inside a cell, a decrease of the CE value corresponds to an increase in the degradation rate and an increase of the CE value indicates a decrease in the degradation rate.

3.3. Identification of aging mechanisms using incremental capacity analysis

In the previous sections, based on cycling data from two types of cells, we have shown that the behavior of long-term CE reveals the degradation rate inside a cell. In this section, we focus on understanding why these two cells exhibit different degradation shapes and digging into the relationships between CE and battery degradation. For this purpose, IC analysis [2], which reveals gradual changes inside cells, is employed here. The IC depicts the relationship of a capacity change associated with a voltage step ($\Delta Q / \Delta V$) during a charge/discharge process. Originally, the IC curve is obtained by charging or discharging a cell at an extremely small portion of a current, such as 1/25C, to guarantee cells operating at "close-to-equilibrium" conditions [25]. Although the battery charging/discharging current is larger for on-board use, it was shown in Refs. [26,27] that, for normal charging and discharging data, the peaks on the IC curve can be still identified and important signatures about battery health state can be revealed. All results presented in this section for the IC analysis are based on 1C discharge data. An easy and accessible way for generating an IC curve was introduced in Ref. [26].

The battery aging mechanism can be understood by observing the evolution of the peaks in the IC curve over the life cycle. LLI (mainly caused by side reactions such as SEI formation and growth, decomposition reactions, lithium plating, etc.), LAM (e.g., material dissolution, particle isolation, electrode delamination, and structural degradation), and an increase of IR (e.g., passive films at the active particle surface and loss of electrical contact within the porous electrode) are three main processes causing battery degradation [1]. These factors can be readily identified via a disproportional decrease in peak intensity (the y-axis of the IC

curve), a proportional decrease in peak intensity, and a shift of peak voltage position (the x-axis of the IC curve), respectively [28]. In the following figures presented in this section, the data are from a representative cell from each dataset (LFP: Cell A1; NMC: Cell B1). Other cells are observed to have qualitatively similar behaviors.

Fig. 4 (c) and (d) respectively show the IC curves of an LFP cell and a NMC cell at four different SOHs. All peaks are numbered for fresh cells. For the convenience of analysis, peak information of the LFP cell and the NMC cell is tabulated in Tables 2 and 3, respectively. From Fig. 4 (c), three peaks can be identified on the IC curve of the fresh LFP cell. Fig. 5 (a) shows the peak voltage position vs. SOH and Fig. 5 (b) shows the peak intensity vs. SOH. A disproportional intensity drop of peak 1 is observed in Fig. 5 (b), which is expected to arise from the LLI process. Peaks 2 and 3, on the contrary, almost do not change in intensity, indicating no obvious LAM existing in LFP cells. From Fig. 5 (a), it is seen that the peak positions of all three peaks shift toward lower voltages from 90% SOH to 80% SOH, indicating a dramatic change of IR. Synchronously, in the discharge voltage vs. capacity curve (Fig. 4 (a)), the end-of-charge point recorded after a rest interval of 5 min also moved to a lower voltage, as a result of the increase of battery IR during the formation and growth of the SEI film, especially from 90% SOH to 80% SOH. We measured IR of these cells after fully discharging state to confirm IC analysis. IR was obtained by applying 10 continuous pulses to the battery and averaging the voltage drop of the pulse, then dividing it by the magnitude of the current pulse. The IR of the LFP cell in Fig. 6 (a) has an increase of 44% from 90% SOH state to 80% SOH. The IR has a slight increase of 4% from 80% SOH to 70% SOH, at which range the peak positions in IC curve slightly moved to lower values. To summarize, in terms of the cycle life tests of commercial LFP cells, the LLI and IR increase are the main sources of the cell aging, while there is almost no aging of the cathode or anode materials.

As to the NMC cell, five dominant peaks can be identified in the IC curve of a fresh NMC cell in Fig. 4 (d), with the highest peak value being 2.45 at 3.33 V. Peak intensity from the NMC cell is much smaller than that from the LFP cell, which is due to the fairly flat plateaus existing in the discharge voltage vs. capacity curve of the
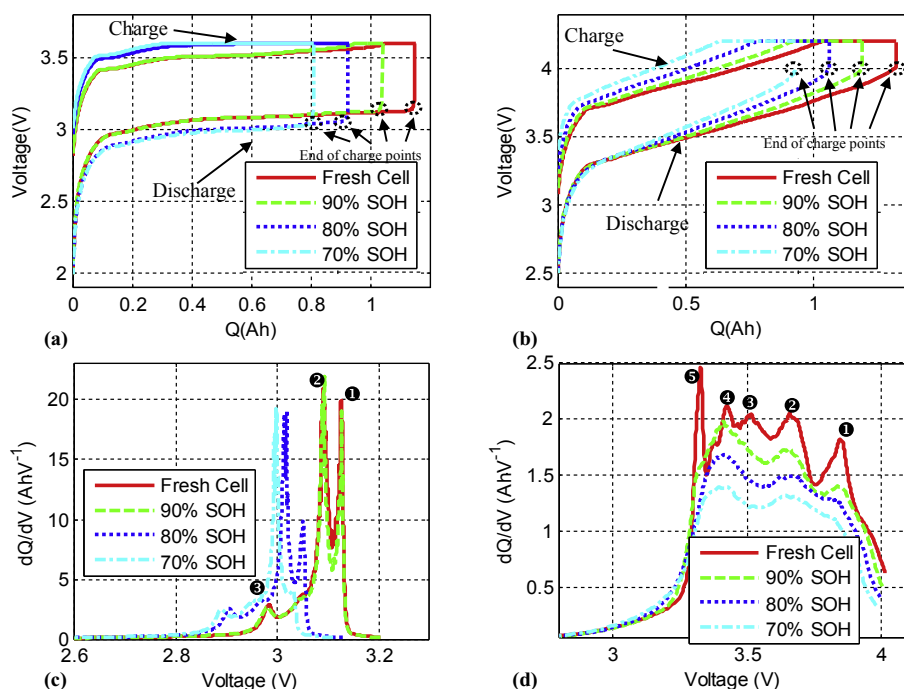
Table 2
Peak information of LFP cells.

SOH	Peak 1		Peak 2		Peak 3	
	Voltage	Intensity	Voltage	Intensity	Voltage	Intensity
100%	3.125	19.99	3.091	20.94	2.982	2.875
90%	3.126	18.93	3.092	21.92	2.98	2.717
80%	3.05	9.804	3.017	19.18	2.904	2.558
70%	3.031	4.094	2.998	19.27	2.889	2.479

LFP cell. Peaks 3 and 5 degenerate so rapidly that no track can be found after the 90% SOH, indicating the existence of the LLI process. From Fig. 7 (b), the intensities of peaks 1, 2, and 4 show fairly good linearity vs. SOH, indicating LAM as a result of structural damage and material loss arising from dissolution of Mn and Fe ions [26]. Possibly, the NMC spinel is considered to release transition metal ions (e.g., Mn^{2+}) that can become incorporated into the anode SEI film, which leads to the acceleration of cell degradation. From Fig. 7 (a), the peak positions of all five peaks are constant, indicating no increase in the battery IR. The measured IR of NMC cells, shown in Fig. 6 (b), keeps steady through most of its lifetime. This is because in modern lithium-ion batteries, better electrolyte additives have reduced internal corrosions that affect IR. Thus, IR does not seem to be a proper life indicator for general purpose; a cell can degrade without IR increase. In this case, in terms of cycle life tests of commercial NMC cells, LLI and LAM are the main sources of the cell aging and there is almost no IR increase.

4. Summary and discussions

4.1. The relationship between aging mechanism, capacity fading, and coulombic efficiency: a summary

We investigated the relationship between the capacity and CE during the long-term cycling of two types of lithium-ion batteries. The aging mechanisms were also investigated using the IC analysis.


Fig. 4. Voltage vs. capacity curves ((a): an LFP cell; (b): a NMC cell) and IC curves ((c): an LFP cell; (d): a NMC cell) at four different SOHs.
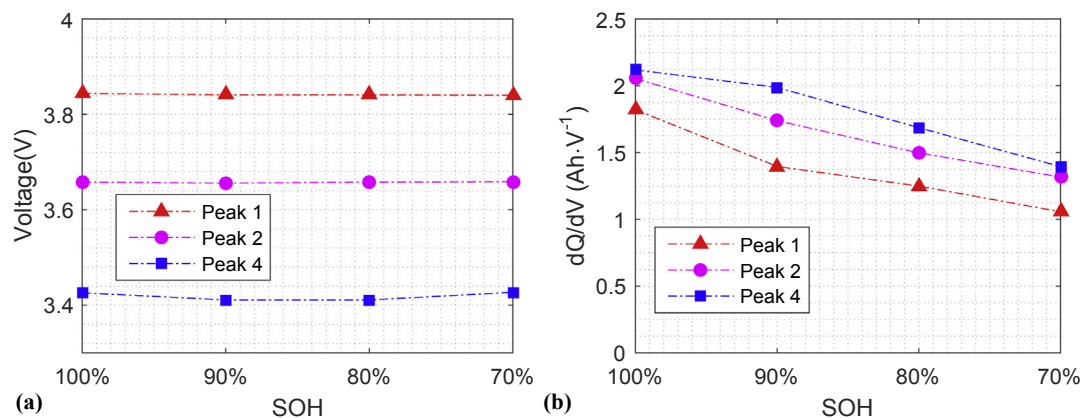
Table 3
Peak information of NMC cells.

SOH	Peak 1		Peak 2		Peak 3		Peak 4		Peak 5	
	Voltage	Intensity	Voltage	Intensity	Voltage	Intensity	Voltage	Intensity	Voltage	Intensity
100%	3.844	1.821	3.658	2.054	3.516	2.045	3.426	2.119	3.328	2.453
90%	3.841	1.396	3.656	1.739			3.411	1.988		
80%	3.841	1.249	3.658	1.497			3.411	1.686		
70%	3.84	1.056	3.659	1.317			3.427	1.394		
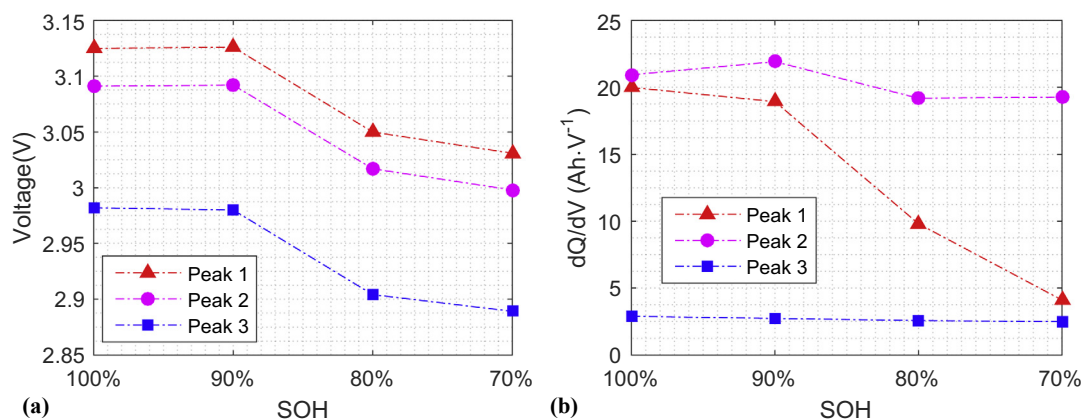
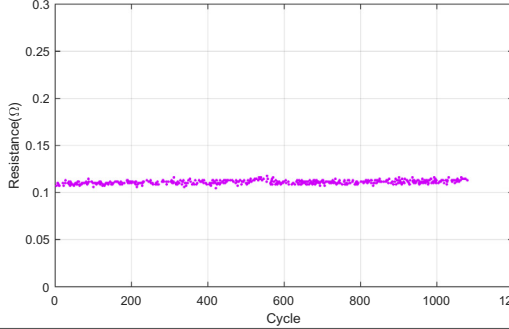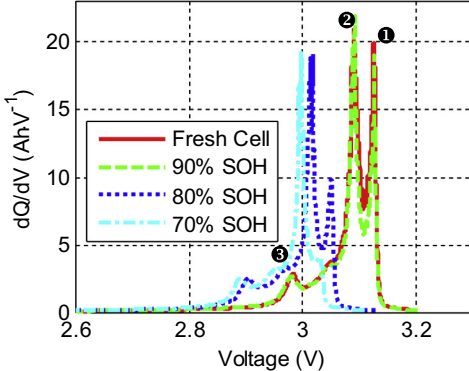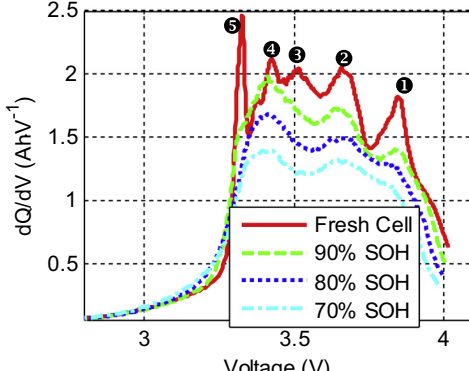**Fig. 5.** Peak information of LFP cells: voltage (a) and intensity (b) vs SOH.
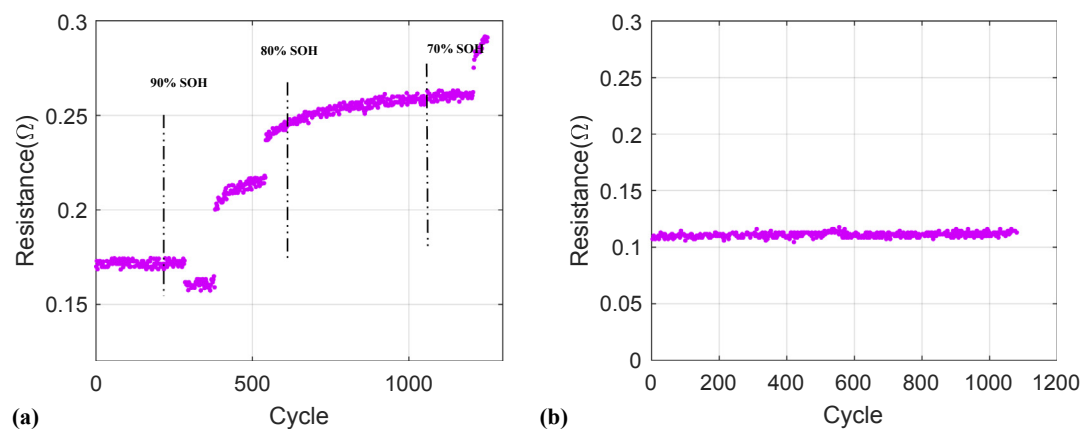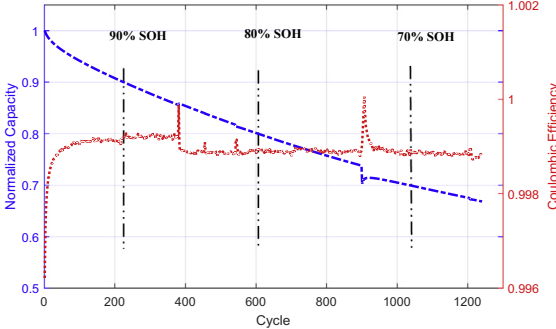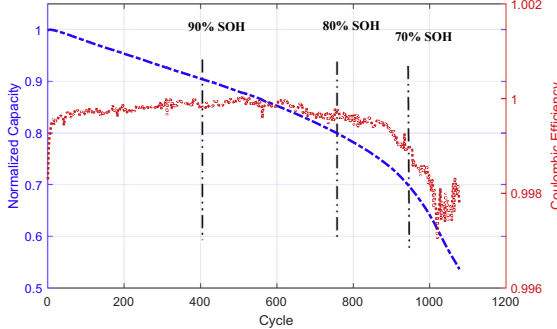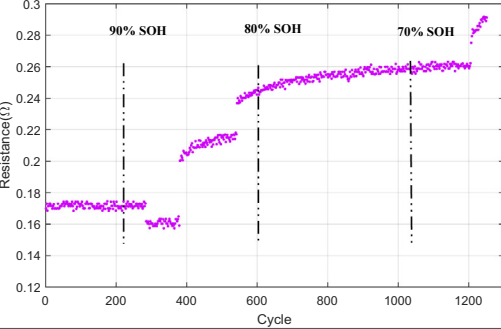
Fig. 6. IR vs. cycle number for cells cycled at 25°C and a discharge rate of 1C: (a) LFP cells, subject to A1; (b) NMC cells, subject to B1.

Fig. 7. Peak information of NMC cells: voltage (a) and intensity (b) vs SOH.

Table 4
Summary of capacity degradation, CE evolution, and aging mechanism.

	LFP cell	NMC cell
Capacity and CE evolution		
IR		
IC curve		
Observation	Stage 1: Fresh to 90% SOH • Observation: CE increases to a stable value. • Aging mechanism: LLI Stage 2: 90% SOH to 80% SOH • Observation: CE drops to a lower level; IR increases by 44%; Peaks move to lower voltages and peak 1 decreases disproportionally. • Aging mechanism: LLI and IR increase State 3: 80% SOH to 70% SOH • Observation: CE remains at a constant level; IR increases by 4%; Peak 1 decreases disproportionally. • Aging mechanism: LLI	Stage 1: Fresh to 80% SOH • Observation: CE increases to a stable value and then remains at a constant level; Peaks 3 and 5 decrease disproportional; • Aging mechanism: LLI Stage 2: 80% SOH ever after • Observation: CE drops dramatically; Peaks 1, 2, and 4 decrease proportional; No IR increase; • Aging mechanism: LAM and LLI

In this section, for a clearer comparison inside a cell, the afore-mentioned experimental observations for a single cell of each battery dataset are tabulated in Table 4.

Three factors including LLI, LAM, and IR increase cause the battery degradation. For LFP cells, LLI and IR increase are two dominating factors. Before 80% SOH, the formation and growth of the SEI film consumes recyclable lithium and results in an increase of IR. After that, the consolidation of the SEI film produces a more

stable interface, reducing the corrosion rate. As a result, LFP cells show a convex degradation behavior, i.e. the degradation rate decreases when cycle number grows. In contrast, for NMC cells, LLI and LAM are two dominating degradation sources. Before 80% SOH, side reactions consume lithium and LLI dominates the aging process. After that, LAM strongly accelerates the battery aging. Consequently, NMC cells show a two-stage concave degradation behavior, where the degradation rate increases when the cycle number increases.
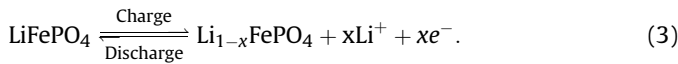
Meanwhile, LLI and LAM bring down the CE value of both types of cells. As to the effect of the IR increase on CE, we do not have enough evidence to draw any conclusion.

Now that cell degradation and CE are affected by LLI, LAM and IR increase, the fact that CE changes in sync with the degradation rate becomes instantly natural, which can be readily observed from Table 4.

4.2. The relationship between coulombic efficiency and battery degradation: an electrochemical perspective

This section provides an explanation for the relationship between CE and battery degradation from an electrochemical perspective. A typical cell is made up of an anode, a cathode, electrolyte and a separator. Fig. 8 shows a schematic of battery operation during charging and discharging. Briefly, during charging, lithium ions migrate from the cathode to the anode, then during discharging, the lithium ions move back to the cathode. Together with lithium ions migration, generated electrochemical reaction makes battery energy transform between chemical energy and electrical energy. Take the following electrochemical reactions of an LFP cell for example.
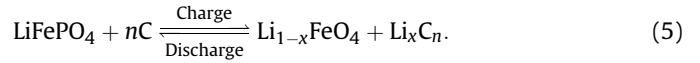
The electrochemical reaction of the LFP cell at the positive electrode is given as follows:

$$\text{LiFePO}_4 \underset{\text{Discharge}}{\overset{\text{Charge}}{\rightleftharpoons}} \text{Li}_{1-x}\text{FePO}_4 + x\text{Li}^+ + xe^-. \quad (3)$$

The electrochemical reaction of the LFP cell at the negative electrode is given as follows:

$$n\text{C} + x\text{Li}^+ + xe^- \underset{\text{Discharge}}{\overset{\text{Charge}}{\rightleftharpoons}} \text{Li}_x\text{C}_n. \quad (4)$$
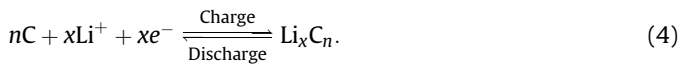
The overall electrochemical reaction of the LFP cell is summarized as follows:

$$\text{LiFePO}_4 + n\text{C} \underset{\text{Discharge}}{\overset{\text{Charge}}{\rightleftharpoons}} \text{Li}_{1-x}\text{FeO}_4 + \text{Li}_x\text{C}_n. \quad (5)$$

In the charging process, the graphite obtains x electrons and reacts with x Li$^+$ ions to form Li$_x$C$_n$. At the same time, LiFePO$_4$ is oxidized to Li$_{1-x}$FePO$_4$ and releases x electrons. Electrons move in an external circuit in the same direction as the lithium ions, while current moves in the opposite direction.

However, removing the lithium ions again during discharging does not reinstate the battery fully. Besides electrochemical reactions which make battery energy transform between chemical energy and electrical energy, there are also some side reactions which take place at an interface between the electrolyte and the electrode at the anode and consume lithium. A loss of effective lithium ions for the electrochemical reactions results in battery performance fading. Denote $N_{d,k}$ as the number of total lithium ions from the anode to the cathode during discharging at cycle k, $N_{c,k}$ as the number of total lithium ions from the cathode to the anode during charging at cycle k, and $N_{l,k}$ as the number of lithium loss at cycle k. Consequently, the following relationship holds on:

$$N_{c,k} = N_{d,k} + N_{l,k}. \quad (6)$$

And the battery degradation rate can be approximated as $N_{l,k}/N_{c,k}$.

On the other hand, CE as the ratio of discharge capacity to charge capacity at cycle k is reformulated by:

$$
\begin{aligned}
\eta_k &= \frac{C_{d,k}}{C_{c,k}} \\
&= \frac{\text{charge quantity of lithium ions back to anode}}{\text{charge quantity of lithium ions from cathode to anode}} \\
&= \frac{N_{d,k}*e}{N_{c,k}*e} = \frac{N_{c,k} - N_{l,k}}{N_{c,k}} = 1 - \frac{N_{l,k}}{N_{c,k}}.
\end{aligned}
\quad (7)
$$

Here, it is found that CE is highly correlated with the battery degradation rate $N_{l,k}/N_{c,k}$ and can be used to indirectly reflect the battery degradation rate.
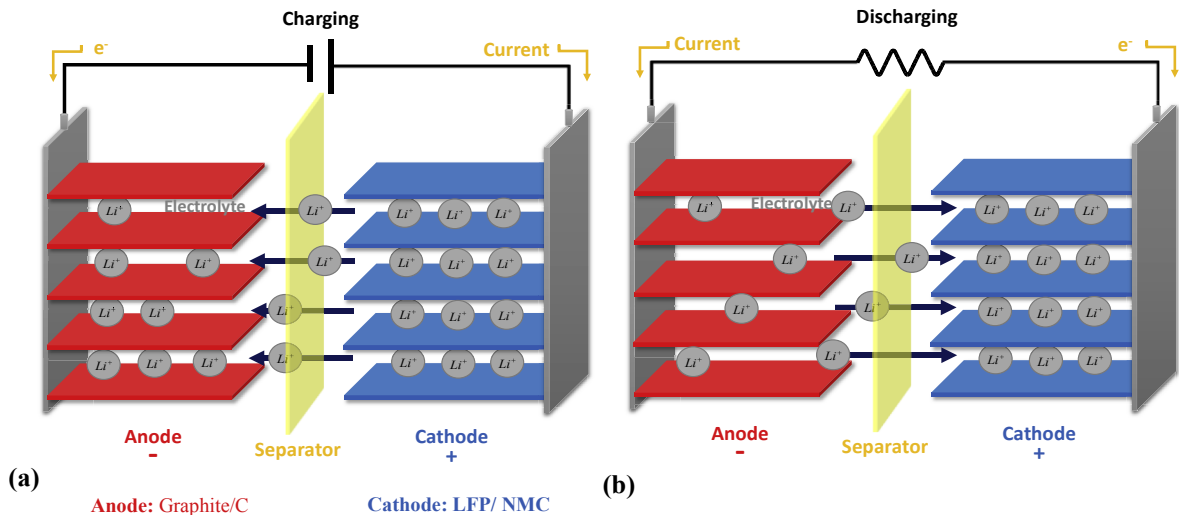

Fig. 8. The operation of a lithium-ion battery during charging and discharging: (a) charging; (b) discharging.
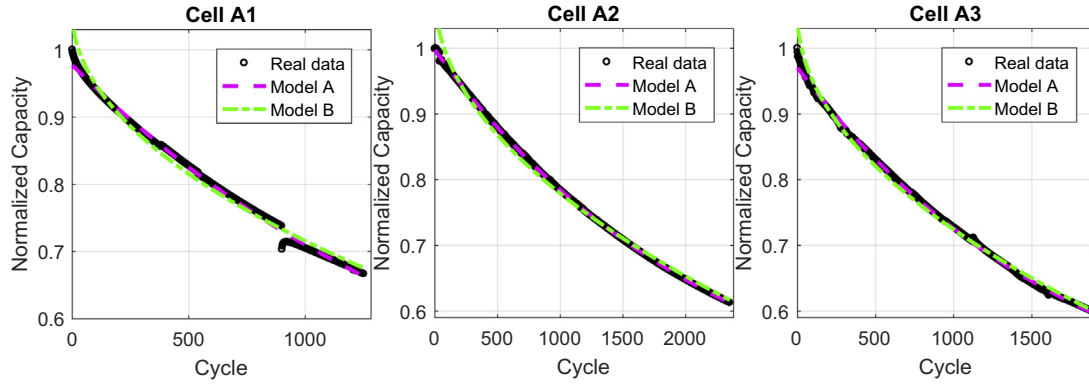
Fig. 9. The fitting ability of two models. Model A: the proposed model; Model B: the square root of time dependency model [30].

4.3. Potential applications of coulombic efficiency

The evolution of CE provides us with significant insight into how battery degradation would behave in a long run. Analyzing CE behavior has potential applications to a battery management system (BMS).

For an LFP cell, of which CE remains constant for most of its life, the cell presents a steady-speed irreversible energy loss. Its capacity then can be considered to decrease by a factor of CE at each cycle. In short, reversible capacity C_k at cycle k can be formulated by C_{k-1} and η_k as follows:

$$C_k = C_{k-1} \cdot \eta_k, \tag{8}$$

C_k then can be iteratively formulated as:

$$C_k = (\eta_k \cdot \eta_{k-1} \cdot \ldots \cdot \eta_1) \cdot C_0, \tag{9}$$

where C_0 is the initial capacity of a cell; the reversible capacity C_k at cycle k can be regarded as the remaining maximum capacity at cycle k.

If we look back to the measured CEs shown in Fig. 2, the CEs over the whole life fluctuate within a small interval. Therefore, we assume $\eta_1 \approx \eta_2 \approx \cdots \approx \eta_k$ and choose it as an unknown parameter, since a precise CE value is extremely hard to obtain [9]. Considering

Equation (9), a model for description of the LFP battery degradation is proposed as follows:

$$\text{Model A:} C_k = \eta^k \cdot \alpha_0 + \alpha_1, \tag{10}$$

where α_0, α_1, and η are the model parameters to be estimated. η indicates the coulombic efficiency of a cell; α_1 is introduced to account for unmodelled factors; and α_0 reflects initial capacity C_0.

The fitting ability of the proposed model is shown in Fig. 9, where it is observed that the proposed model can well capture the convex capacity degradation of LFP cells. In this manner, CE can be employed as a promising variable to model the loss of LFP battery capacity. And the CE-based model would help improve the accuracy of on-board battery capacity estimation. We will elaborate the proposed model and its applications in capacity estimation in our future work.

For an NMC cell, the behavior of CE over a long-term battery life indicates some important degradation changes inside the cell. For instance, the reflection point of the capacity degradation curve coincides with a dramatic decrease of the CE curve (Use Cell B1 as an example in Fig. 10). Warnings about accelerated degradation can be issued once a drastic CE drop is detected. A statistical quality control method, such as exponential weighted moving average [29], etc., can be used to detect aging.
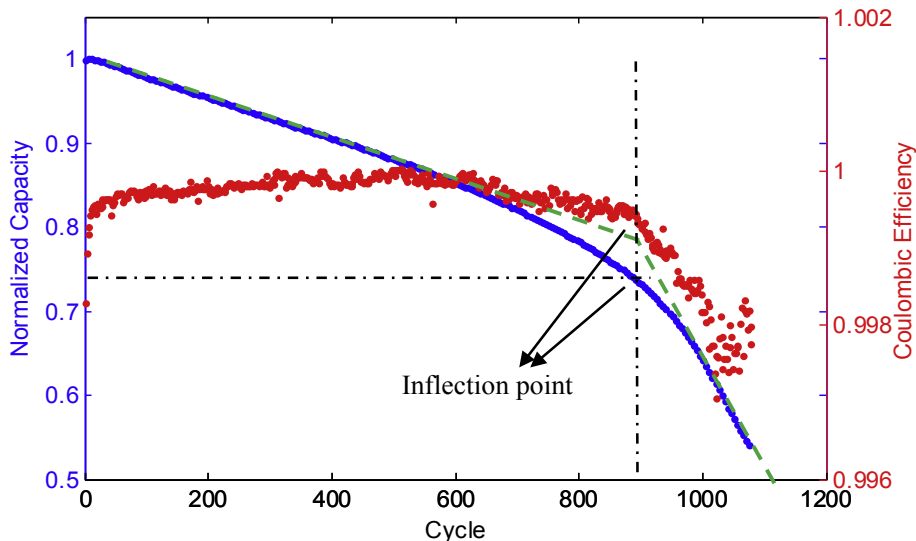

Fig. 10. Capacity degradation and CE evolution of Cell B1 in the constant current tests.

5. Conclusions

In this paper, based on the data collected from the cycle life tests of two types of mainstream commercial lithium-ion cells including LFP cells and NMC cells, we experimentally investigated the long-term CE evolution and its correlation with the battery degradation. Our findings are summarized as follows.

Firstly, it was observed that LFP cells and NMC cells exhibit two distinct aging behaviors. The degradation curves of LFP cells have a typical convex shape, while those of NMC cells represent a two-phase concave degradation behavior. Secondly, the aging mechanisms of these two types of batteries revealed by the IC analysis show that LLI and IR increase are two main aging factors for LFP cells, while LLI and LAM are two main aging sources for NMC cells. Thirdly, according to the experimental observations and theoretical analysis, it was discovered that the long-term CE evolution has a strong and close relationship with the battery degradation, and the long-term CE evolution can be used to indicate the degradation rate inside a cell. More specifically, a stable CE curve corresponds to a constant degradation rate, while a sharp decrease of the CE curve indicates an increased rate of degradation.

Further, the aforementioned findings are helpful for users to improve BMS performance. Some recommendations for our future studies are given as follows. Firstly, CE as an indicator of battery degradation rate can be employed as a promising variable to model the loss of LFP battery capacity. The CE-based model proposed in this paper would be helpful to accurately estimate on-board battery capacity. Secondly, on-line monitoring of CE value using statistical quality control methods can help estimate the health state of a battery and provide early warnings for accelerated degradation.

References

[1] Kassem M, Bernard J, Revel R, Pelissier S, Duclaud F, Delacourt C. Calendar aging of a graphite/LiFePO 4 cell. J Power Sources 2012;208:296–305.
[2] Dubarry M, Liaw BY. Identify capacity fading mechanism in a commercial LiFePO$_4$ cell. J Power Sources 2009;194(1):541–9.
[3] Vetter J, Novák P, Wagner M, Veit C, Möller K-C, Besenhard J, et al. Ageing mechanisms in lithium-ion batteries. J Power Sources 2005;147(1):269–81.
[4] Smith A, Burns J, Dahn J. A high precision study of the Coulombic efficiency of Li-ion batteries. Electrochem Solid-State Lett 2010;13(12):A177–9.
[5] Ohzuku T, Ueda A, Yamamoto N, Iwakoshi Y. Factor affecting the capacity retention of lithium-ion cells. J Power Sources 1995;54(1):99–102.
[6] Gyenes B, Stevens D, Chevrier V, Dahn J. Understanding anomalous behavior in coulombic efficiency measurements on Li-Ion batteries. J Electrochem Soc 2015;162(3):A278–83.
[7] Burns J, Kassam A, Sinha N, Downie L, Solnickova L, Way B, et al. Predicting and extending the lifetime of Li-ion batteries. J Electrochem Soc 2013;160(9): A1451–6.
[8] Ng KS, Moo C-S, Chen Y-P, Hsieh Y-C. Enhanced coulomb counting method for estimating state-of-charge and state-of-health of lithium-ion batteries. Appl Energy 2009;86(9):1506–11.
[9] Zheng Y, Ouyang M, Lu L, Li J, Zhang Z, Li X. Study on the correlation between state of charge and coulombic efficiency for commercial lithium ion batteries. J Power Sources 2015;289:81–90.
[10] Wang J, Cao B, Chen Q, Wang F. Combined state of charge estimator for electric vehicle battery pack. Control Eng Pract 2007;15(12):1569–76.
[11] Smith A, Trussler S, Dahn J. Precision measurements of the coulombic efficiency of lithium-ion batteries and of electrode materials for lithium-ion batteries. J Electrochem Soc 2010;157(2):A196–202.
[12] Bond T, Burns J, Stevens D, Dahn H, Dahn J. Improving precision and accuracy in coulombic efficiency measurements of Li-ion batteries. J Electrochem Soc 2013;160(3):A521–7.
[13] Yang F, Wang D, Xing Y, Tsui K-L. Prognostics of Li (NiMnCo) O$_2$-based lithium-ion batteries using a novel battery degradation model. Microelectron Reliab 2017;70:70–8.
[14] Xu J, Deshpande RD, Pan J, Cheng Y-T, Battaglia VS. Electrode side reactions, capacity loss and mechanical degradation in lithium-ion batteries. J Electrochem Soc 2015;162(10):A2026–35.
[15] Deshpande RD, Ridgway P, Fu Y, Zhang W, Cai J, Battaglia V. The limited effect of VC in graphite/NMC cells. J Electrochem Soc 2015;162(3):A330–8.
[16] Yang F, Xing Y, Wang D, Tsui K-L. A comparative study of three model-based algorithms for estimating state-of-charge of lithium-ion batteries under a new combined dynamic loading profile. Appl Energy 2016;164:387–99.
[17] Lu L, Han X, Li J, Hua J, Ouyang M. A review on the key issues for lithium-ion battery management in electric vehicles. J Power Sources 2013;226:272–88.
[18] Andrea D. Battery management systems for large lithium ion battery packs. Artech House; 2010.
[19] Hunt G. USABC electric vehicle battery test procedures manual. Washington, DC, USA: United States Department of Energy; 1996.
[20] Deshpande R, Verbrugge M, Cheng Y-T, Wang J, Liu P. Battery cycle life prediction with coupled chemical degradation and fatigue mechanics. J Electrochem Soc 2012;159(10):A1730–8.
[21] Fathi R, Burns J, Stevens D, Ye H, Hu C, Jain G, et al. Ultra high-precision studies of degradation mechanisms in aged LiCoO$_2$/graphite Li-ion cells. J Electrochem Soc 2014;161(10):A1572–9.
[22] Liu W, Delacourt C, Forgez C, Pelissier S. Study of graphite/NCA Li-ion cell degradation during accelerated aging tests—Data analysis of the SIMSTOCK project. In: 2011 IEEE vehicle power and propulsion conference. IEEE; 2011. p. 1–6.
[23] He W, Williard N, Osterman M, Pecht M. Prognostics of lithium-ion batteries based on dempster–shafer theory and the Bayesian monte Carlo method. J Power Sources 2011;196(23):10314–21.
[24] Han X, Ouyang M, Lu L, Li J. Cycle life of commercial lithium-ion batteries with lithium titanium oxide anodes in electric vehicles. Energies 2014;7(8): 4895–909.
[25] Dubarry M, Truchot C, Liaw BY. Synthesize battery degradation modes via a diagnostic and prognostic model. J Power Sources 2012;219:204–16.
[26] Han X, Ouyang M, Lu L, Li J, Zheng Y, Li Z. A comparative study of commercial lithium ion battery cycle life in electrical vehicle: aging mechanism identification. J Power Sources 2014;251:38–54.
[27] Weng C, Sun J, Peng H. A unified open-circuit-voltage model of lithium-ion batteries for state-of-charge estimation and state-of-health monitoring. J Power Sources 2014;258:228–37.
[28] Dubarry M, Liaw BY. Identify capacity fading mechanism in a commercial LiFePO$_4$ cell. J Power Sources 2009;194(1):541–9.
[29] Lucas JM, Saccucci MS. Exponentially weighted moving average control schemes: properties and enhancements. Technometrics 1990;32(1):1–12.
[30] Wang J, Liu P, Hicks-Garner J, Sherman E, Soukiazian S, Verbrugge M, et al. Cycle-life model for graphite-LiFePO$_4$ cells. J Power Sources 2011;196(8): 3942–8.